CORA Cork Open Research Archive
Cartlann Taighde Oscailte Chorcaí

Title	Refractive index dynamics of InAs/GaAs quantum dots
Authors	Crowley, Mark T.;Houlihan, John;Piwonski, Tomasz;O'Driscoll, Ian;Williams, David P.;O'Reilly, Eoin P.;Uskov, Alexander V.;Huyet, Guillaume
Publication date	2013
Original Citation	Crowley, M. T., Houlihan, J., Piwonski, T., O'Driscoll, I., Williams, D. P., O'Reilly, E. P., Uskov, A. V. and Huyet, G. (2013) 'Refractive index dynamics of InAs/GaAs quantum dots', Applied Physics Letters, 103(2), pp. 021114. doi: 10.1063/1.4813472
Type of publication	Article (peer-reviewed)
Link to publisher's version	http://aip.scitation.org/doi/abs/10.1063/1.4813472 - 10.1063/1.4813472
Rights	© 2013 AIP Publishing LLC..This article may be downloaded for personal use only. Any other use requires prior permission of the author and AIP Publishing. The following article appeared in Crowley, M. T., Houlihan, J., Piwonski, T., O'Driscoll, I., Williams, D. P., O'Reilly, E. P., Uskov, A. V. and Huyet, G. (2013) 'Refractive index dynamics of InAs/GaAs quantum dots', Applied Physics Letters, 103(2), pp. 021114 and may be found at http://aip.scitation.org/doi/abs/10.1063/1.4813472
Download date	2026-11-06 04:53:09
Item downloaded from	https://hdl.handle.net/10468/4283

UCC
University College Cork, Ireland
Coláiste na hOllscoile Corcaigh

Refractive index dynamics of InAs/GaAs quantum dots

M. T. Crowley, J. Houlihan, T. Piwonski, I. O'Driscoll, D. P. Williams, E. P. O'Reilly, A. V. Uskov, and G. Huyet

Citation: Appl. Phys. Lett. **103**, 021114 (2013); doi: 10.1063/1.4813472
View online: http://dx.doi.org/10.1063/1.4813472
View Table of Contents: http://aip.scitation.org/toc/apl/103/2
Published by the American Institute of Physics

Articles you may be interested in

Refractive index dynamics of quantum dot based waveguide electroabsorbers
Applied Physics Letters **97**, 051107 (2010); 10.1063/1.3476347

Gain and refractive index dynamics in p-doped InAs quantum dash semiconductor optical amplifiers
Applied Physics Letters **109**, 031102 (2016); 10.1063/1.4955460



Refractive index dynamics of InAs/GaAs quantum dots

M. T. Crowley,[1] J. Houlihan,[2] T. Piwonski,[1,3] I. O'Driscoll,[1,3] D. P. Williams,[1,3] E. P. O'Reilly,[1] A. V. Uskov,[4] and G. Huyet[1,3]
[1]*Tyndall National Institute, Lee Maltings, Cork, Ireland*
[2]*Department of Computing, Maths and Physics, Waterford Institute of Technology, Waterford, Ireland*
[3]*Department of Applied Physics, Cork Institute of Technology, Cork, Ireland*
[4]*P. N. Lebedev Physical Institute, Leninsky pr. 53, 117924 Moscow, Russia*

(Received 11 January 2013; accepted 25 June 2013; published online 11 July 2013)

The refractive index dynamics of an InAs/InGaAs/GaAs dots-in-a-well semiconductor optical amplifier is calculated and compared with experimental results. The fast and slow recovery timescales together with the behaviour with increasing injection are reproduced and explained in terms of the density of carriers available in upper quantum dot and continuum states. Also, a Coulomb-mediated shift of the dot susceptibility is suggested as responsible for the fast recovery of the phase. © *2013 AIP Publishing LLC*. [http://dx.doi.org/10.1063/1.4813472]

The unique properties of quantum dot (QD) based photonic materials have been intensively studied and have enabled performance improvements, for particular applications, over bulk and quantum well based structures.[1] Early simulation work suggested that QD based semiconductor optical amplifiers (SOAs) could realise high speed pattern free amplification[2] and improved nonlinear interferometers[3] where the unique carrier dynamics and decoupling of phase and gain were the key advantages. Subsequent pump probe measurements of QD SOA phase dynamics at 1.3 μm confirmed the dominant role of continuum states in the refractive index dynamics.[4] More recently, detailed calculations on the influence of pump wavelength on gain and refractive index dynamics were presented.[5] We calculate, and directly compare with experiment, the refractive index dynamics at 1.3 μm resulting from strong perturbations resonant either with the QD ground state (GS) or excited state (ES) transition energy.

Optical emission was measured from the dots-in-a-well (DWELL) SOA structure at 0.94 eV and 0.995 eV for the GS and first ES of the QD ensemble. Higher energy emission was observed at 1.27 eV and 1.33 eV due, respectively, to higher order dot states merging with the bandedge states of the InGaAs QW and to transitions involving fully delocalised QW states.[6,7] A QD model was constructed to match these emission energies, including the QD electron/hole GS and ES levels as well as the electron/hole states for the QW emission peaks (C1 and C2). An 8-band **k.P** model was then used to calculate peak values of the optical cross-sections for the GSe-GSh, ESe-ESh, C1e-C1h, and C2e-C2h transitions of $2\cdot10^{-19}\mathrm{m}^2$, $3.5\cdot10^{-19}\mathrm{m}^2$, $5.4\cdot10^{-19}\mathrm{m}^2$, and $5.4\cdot10^{-19}\mathrm{m}^2$, respectively.[8] The hole states involved in possible "crossed" transitions with the QD GS and ES electrons are lumped with the C1h level and modeled as GSe-C1h and as ESe-C1h, both with an assumed peak optical cross-section of $1\cdot10^{-19}\mathrm{m}^2$.[9] The relative density of states (DOS) associated with the different levels are taken as 1:2:14:14 and 1:2:30:30 for electrons and holes, respectively, and the calculated energy difference between the QD GS and ES electron (hole) states is 40(20) meV. The real and imaginary parts of the susceptibility for each of these transitions are related by a Hilbert transformation and can be written in closed form as shown in Eqs. (4) and (5) below following the density matrix formulation.[10]

The dynamics of the various electron/hole populations resolved along the SOA (z-direction) are described by the following equation:

$$\frac{\partial n_j^{e(h)}}{\partial t} = \left(\frac{JA}{q}\right)_{j=C2} + \sum_{i,i\neq j}\frac{n_i^{e(h)}}{\tau_{i\to j}}\left(1-f_j^{e(h)}\right) - \sum_{i,i\neq j}\frac{n_j^{e(h)}}{\tau_{j\to i}}\left(f_i^{e(h)}\right) - \frac{\sqrt{n_j^e n_j^h}}{\tau_r} - g_{mod}^{inter} v_g A_{wg} LS[z,t], \quad (1)$$

where $e(h)$ refers to the electron (hole) case, j indexes the level type (GS,ES,C1,C2), J is the effective injection current density (this term is for the C2 level only), A is the area of the active region, and q is the electronic charge. Carrier capture into level j is accounted for by the second term and involves the occupation probability of the state f_j and the carrier density (n_i) and capture time from state i to j ($\tau_{i\to j}$). Carrier escape from level j is described in the third term which involves the occupation probability of the state f_i together with the carrier density (n_j) and escape time from state j to i ($\tau_{j\to i}$). Both escape and capture are assumed to follow a cascaded relaxation mechanism and other relaxation pathways are neglected (following the conclusions in Ref. 11).

The capture rates are assumed to be identical for electrons and holes and are taken to be 10 ps, 2 ps, and 0.5 ps for capture from C2 to C1, C1 to ES, and ES to GS, respectively. These have been chosen to match typical timescales extracted from pump-probe studies.[4] The corresponding escape times are then determined using

$$\tau_{i\to j} = \tau_{j\to i}\frac{D_i}{D_j}Exp\left[\frac{(\Delta E)_{ij}}{k_B T}\right], \quad (2)$$

where D_i is the relative DOS of state i, yielding escape times for electrons (holes) of 3.5(0.8)ps from GS to ES, 121(2.6)ps from ES to C1, and 53(23)ps for C1 to C2. The resulting faster hole dynamics stem from the closer level separations in the valence band.[12] Equation (2) constrains the carrier

 © 2013 AIP Publishing LLC

distributions to approach a Fermi-Dirac thermal distribution. The τ_r term in Eq. (1) describes the carrier lifetime; we assume a carrier recombination lifetime of 300 ps in all levels. Small-signal carrier populations for various currents are presented in Table I.

The final term in Eq. (1) involves the photon density $S[z,t]$ and describes stimulated emission involving both resonant and "crossed" transitions as described earlier. Here, ν_g is the group velocity, L is the length of the waveguide, A_{wg} is the effective optical cross-section of the waveguide, and g_{mod}^{inter} is the modal gain. The optical pump and probe pulse envelopes are separately propagated in a retarded time frame along the SOA according to

$$\frac{\partial S[z,t]}{\partial t} = (g_{mod}^{inter}[\omega,z,t] - \alpha_i)S[z,t], \tag{3}$$

where in the case of the probe, a delayed time is used to trace the effect of the pump pulse on the system.[2] Here, α_i is the internal loss (set to $3\,\mathrm{cm}^{-1}$), ω is the frequency, and the modal gain is given by

$$g_{mod}^{inter} = \frac{\Gamma l}{a}\sum_{i,m,n}\sigma_{i,mn}^{Im}[\omega](f_{i,m}+f_{i,n}-1), \tag{4}$$

where Γ is the overlap of the optical field with the active region, l is the number of dot layers, and a is the mean height of a dot. The sum i extends over all dots in one unit area in a single dot layer. In practice, the summation is replaced by integration and includes the effect of inhomogeneous broadening as outlined in Eqs. (6) and (7) in Ref. 2. The sum over m and n pairs includes all contributing direct and "crossed" transitions, $\sigma_{i,mn}^{Im}$ being the imaginary part of the optical cross-section corresponding to a particular transition and $f_{i,m}$ and $f_{i,n}$ the respective electron and hole occupancies. A very similar expression holds for the interband contribution to the refractive index, i.e.,

$$\eta_{mod}^{inter} = \frac{\Gamma l}{a}\frac{c}{8\pi^2\omega}\sum_{i,m,n}\sigma_{i,mn}^{Re}[\omega](f_{i,m}+f_{i,n}-1), \tag{5}$$

where c is the vacuum speed of light. The real and imaginary parts of the optical cross-section are calculated from

TABLE I. Calculated equilibrium carrier populations per dot for an injected current of 30 mA, 100 mA, and 180 mA, which give a total number of electrons (e) and holes (h) injected per dot of 2.85, 6.5, and 10.1, respectively. C1 refers to the dense distribution of higher order dot states merging with the continuum states, while C2 refers to delocalised carrier states.

Level	30 mA	100 mA	180 mA
GSe	1.46	1.99	2.00
GSh	0.89	1.47	1.70
ESe	1.33	3.86	3.98
ESh	1.08	2.23	2.88
C1e	0.008	0.51	3.24
C1h	0.60	2.02	3.97
C2e	0.002	0.13	0.88
C2h	0.23	0.77	1.55

$$\sigma_{i,mn}^{Re}[\omega] = \frac{2\pi\mu_{i,mn}^2\omega_{i,mn}T_{i,mn}}{c\eta_b\epsilon_0 h}\frac{(\omega_{i,mn}-\omega)}{1+\left((\omega_{i,mn}-\omega)T_{i,mn}\right)^2}, \tag{6}$$

and

$$\sigma_{i,mn}^{Im}[\omega] = \frac{2\pi\mu_{i,mn}^2\omega_{i,mn}T_{i,mn}}{c\eta_b\epsilon_0 h}\frac{1}{1+\left((\omega_{i,mn}-\omega)T_{i,mn}\right)^2}, \tag{7}$$

where $\mu_{i,mn}$ is the dipole moment of the transition, $T_{i,mn}$ is its dephasing time ($=2/\gamma_{hom}$ in terms of the homogeneous broadening), $\omega_{i,mn}$ is the transition frequency, η_b is the background index ($=3.5$), h is Planck's constant, and ϵ_0 is the vacuum permittivity. Thus, the total induced phase change is calculated by combining the effect of the interband transitions for the given dot structure and also includes the intraband excitations of each electron and hole population using the Drude model[3,13] i.e.,

$$\Delta\phi = \frac{4\pi^2\omega L}{c}\left[\sum_j \eta_{mod}^{inter} + \sum_{m,n}\eta_{mod}^{intra}\right]. \tag{8}$$

The homogeneous broadening for band to band transitions is taken as 13 meV and the inhomogeneous broadening of transitions as $h\gamma_{inhomo}/2\pi = 40$ meV.[8] The GS absorption based on these values for a 6 layer device is $30\,\mathrm{cm}^{-1}$, while the net gain is only $8\,\mathrm{cm}^{-1}$. According to the device used experimentally, we assume $L=3$ mm and 6 layers of DWELLs with an areal dot density of $3\cdot10^{10}\,\mathrm{cm}^{-2}$ per layer.[6]

The carrier populations (averaged over the inhomogeneously broadened dot ensemble) are listed for different injection levels in Table I. The measured energy of the pump pulse before coupling to the SOA waveguide is 3.5 pJ. As it is difficult to precisely determine the coupling losses in the experiment, the input pulse energy in the model is fitted (0.75 pJ) so that the phase response seen by the probe at 30 ps agrees closely with the measured value for the GS pump/GS probe case at 30 mA. The phase dynamics are then calculated at 100 mA and 180 mA for pump pulses resonant with GS and ES transition energies and the results compared with the experimental response.

Figure 1(a) shows the measured phase responses at injection currents of 30 mA (red plot), 100 mA (blue lines), and 180 mA (black lines) for the case where the pump pulse is at the GS peak (solid lines) and ES peak (dashed lines). The currents used correspond to ~1.8, ~ 5.9, and ~10.6 times the measured GS transparency current and ~1.8 and ~3.3 times the measured ES transparency current, respectively (see Ref. 14 for more details). The main trend apparent in this figure is that the difference in phase response between 100 mA and 180 mA is much greater when pumping at the ES (dashed lines) than when it is pumping at the GS (solid lines). Also, the 180 mA GS and ES and 100 mA GS cases are all very similar.

Figure 1(b) displays the calculated phase transients when the probe pulse is tuned to the maximum of the GS gain spectrum. The model qualitatively reproduces the main trends in the measured phase transients. The relative magnitudes of the phase are very similar to the experimental case

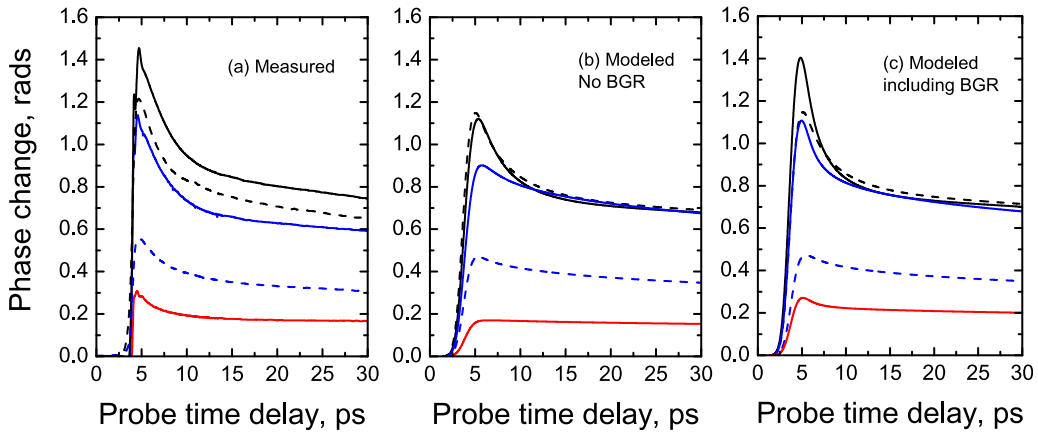


FIG. 1. (a) Measurements of QD SOA phase at currents of 30 mA (red), 100 mA (blue), and 180 mA (black) for GS pump (solid lines) and ES pump (dashed lines). (b) Calculations without band-gap renormalisation due to QD carriers. (c) Calculations including bandgap renormalisation due to QD carriers.

after 10 – 15ps and, indeed, pumping at the ES results in a greater change in phase response with increasing current (in comparison to pumping at the GS). Also, the 180 mA GS and ES and 100 mA GS cases are all very similar, as in the experimental case. The physical mechanism behind these observations is apparent on consideration of the various level occupancies shown in Table I and can be attributed to the availability or lack of a carrier reservoir at higher energy relative to the pump pulse. For the GS, the availability of carriers in the ES means that the phase differential is not large going from 100 mA to 180 mA. In contrast for the ES, the population of the C1 levels (which act as a reservoir for the ES) show a significant increase over this current range. Note that the GS does not act as a reservoir for the ES due to the larger escape time compared with the capture time from C1 to ES.

While reproducing the qualitative behaviour, the model does not capture the ultrafast portion of the dynamics (<10 ps). In fact, as the injection increases, the ultrafast component makes up ~50% of the signal after 30 ps, up from ~30% at 30 mA. This dependence on injection suggests a role for carrier-carrier interactions. Previous work based on time-resolved photoluminescence has identified a blue shift in the QD emission spectrum of tens of meV.[15] In addition, a shift of 8 meV due to band filling was deduced by analysis of

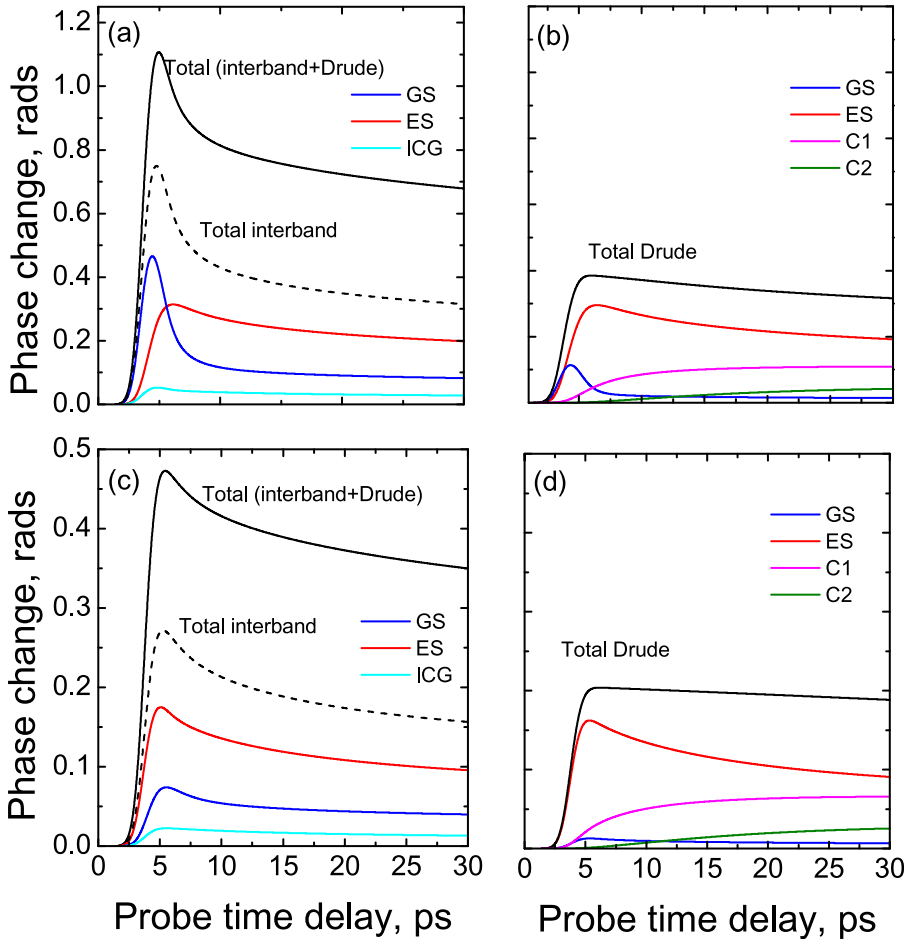


FIG. 2. Calculations at 100 mA for pumping in the GS (top panels) and ES (bottom panels). Contributions from interband (left panels) and Drude (right panels) transitions are shown for carriers in the GS (blue), ES (red), C1 (magenta), C2 (green), and the interband contribution due to the crossed transitions ICG (cyan). The C1 and C2 interband contributions are very small and not shown.

the observed GS peak absorption and gain at 2.2e-h pairs per dot.[16] This is similar to the dot population for the 30 mA case in this work (see Table I).

For higher initial injection levels, where there is a population in the C1 levels, the reduction of that population has been shown to shift the dot GS emission by up to 20 meV.[15] The observed shifts for the ES are usually much smaller.[15,17] Thus, we might expect that band gap renormalization (BGR) resulting from the Coulomb interaction between charge carriers can cause such a blue shift in response to an intense ultra short pulse. At 10e-h pairs per dot, the carrier density per dot is $\sim 6.35 \cdot 10^{18} \mathrm{cm}^{-3}$, assuming a cube shaped dot of $\sim 15 \mathrm{nm}^3$. Based on the model of Wolff[18] which assumes that band gap shrinkage in a material varies as the cube root of the carrier density or the average interparticle spacing we have the following expression:

$$\Delta E_{BGS} = \frac{-e}{2\pi\epsilon_0\epsilon_s}\left(\frac{3}{\pi}\right)^{1/3} n^{1/3}, \tag{9}$$

where ϵ_s is the static dielectric constant of the semiconductor and n is the total carrier density of the dot levels (GS+ES+C1). This expression has previously been used to model the carrier-induced refractive index in bulk GaAs, InP and alloys of InGaAsP lattice-matched to InP.[19] Figure 1(c) shows the same calculation as shown in part (b) with the addition of the carrier density dependent blue-shift of the susceptibility function. The ultrafast component of the phase recovery is enhanced and the overall dynamics is much closer to the experimental case than previously. Physically, the BGR results in the GS resonance shifting from the centre frequency of the pulse. Consequently the GS transition (and, in particular, its fast component) contributes much more to the phase shift than the case where the GS remained on resonance with the pulse and positive and negative phase contributions from the GS cancelled.

To investigate the dynamics further, Figure 2 shows the calculated GS phase contribution from each transition at 100 mA for both GS and ES pumping. At this injection level, GS pumping results in almost twice as much phase change than ES pumping for each energy level (see values at 30 ps) due to the increased number of carriers available for stimulated emission as the pump pulse propagates. Under GS pumping, once GS carriers are depleted, ES carriers can quickly relax into vacated GS levels within the pulse duration to be available for further stimulated emission.[2] In contrast, under ES pumping, the C1 to ES and GS to ES channels are not fast enough to replenish exhausted carriers within the duration of the pulse. Thus, more GS and ES states are vacated by the GS pump than the ES one; these are then replenished from the C1 and C2 states over longer timescales. This effect is particularly noticeable in the C1 Drude contribution where the C1 hole population is more heavily depleted over 30 ps under GS rather than ES pump conditions (see Table I for steady state population levels). As the current increases to 180 mA, the changing steady state population levels increase the ES gain, resulting in less difference between the number of carriers removed under GS and ES pumping schemes. As a result, similar phase dynamics occurs in both cases.

In conclusion, we have reproduced measurements of the GS phase dynamics at 1.3μm in InAs/GaAs QD SOAs when pumped in both the GS and ES. Band gap renormalization is identified as the cause of the increased fast phase component that occurs for GS pumping, while the difference between GS and ES pumping at lower currents is connected to the steady state level populations.

This work was supported in part by Science Foundation Ireland (Contract No. 06/IN.1/I90).

[1]M. T. Crowley, N. A. Naderi, H. Su, F. Grillot, and L. F. Lester, *Advances in Semiconductor Lasers* (Academic, New York, 2012), Chap. 10.
[2]A. V. Uskov, T. W. Berg, and J. Mork, IEEE J. Quantum Eletron. **40**, 306 (2004).
[3]A. V. Uskov, E. P. O'Reilly, R. J. Manning, R. P. Webb, D. Cotter, M. Laemmlin, N. N. Ledentsov, and D. Bimberg, IEEE Photonics Technol. Lett. **16**, 1265 (2004).
[4]I. O'Driscoll, T. Piwonski, C. F. Schleussner, J. Houlihan, G. Huyet, and R. J. Manning, Appl. Phys. Lett. **91**, 071111 (2007).
[5]J. Kim, C. Meuer, D. Bimberg, and G. Eisenstein, Semicond. Sci. Technol. **26**, 014007 (2011).
[6]T. Piwonski, I. O'Driscoll, J. Houlihan, G. Huyet, R. J. Manning, and A. V. Uskov, Appl. Phys. Lett. **90**, 122108 (2007).
[7]M. T. Crowley, N. Patel, T. A. Saiz, M. El Emawy, T. A. Nilsen, N. A. Naderi, S. D. Mukherjee, B. O. Fimland, and L. F. Lester, Semicond. Sci. Technol. **27**, 065011 (2012).
[8]M. T. Crowley, I. P. Marko, N. F. Masse, A. D. Andreev, S. Tomic, S. J. Sweeney, E. P. O'Reilly, and A. R. Adams, IEEE J. Sel. Top. Quantum Electron. **15**(3), 799–807 (2009).
[9]M. T. Crowley, A. D. Andreev, T. Piwonski, J. Houlihan, E. P. O'Reilly, and G. Huyet, Phys. Status Solidi B **246**, 868–871 (2009).
[10]M. Asada and Y. Suematsu, IEEE J. Quantum Electron. **21**, 434–442 (1985).
[11]N. Majer, K. Lüdge, and E. Scholl, Phys. Rev. B **82**, 235301 (2010).
[12]E. A. Viktorov, P. Mandel, Y. Tanguy, J. Houlihan, and G. Huyet, Appl. Phys. Lett. **87**, 053113 (2005).
[13]C. H. Henry, R. A. Logan, and K. A. Bertness, J. Appl. Phys. **52**, 4457–4461 (1981).
[14]I. O'Driscoll, T. Piwonski, J. Houlihan, G. Huyet, R. J. Manning, and B. Corbett Appl. Phys. Lett. **91**, 263506 (2007).
[15]Z. L. Yuan, E. R. A. D. Foo, J. F. Ryan, D. J. Mowbray, M. S. Skolnick, and M. Hopkinson, Phys. Status Solidi A **178**, 345 (2000).
[16]I. O'Driscoll, M. Hutchings, P. M. Smowton, and P. Blood, Appl. Phys. Lett. **97**, 141102 (2010).
[17]F. Quochi, M. Dinu, L. N. Pfeiffer, K. W. West, C. Kerbage, R. S. Windeler, and B. J. Eggleton, Phys. Rev. B **67**, 235323 (2003).
[18]P. A. Wolff, Phys. Rev. **126**, 405 (1962).
[19]B. R. Bennett, R. A. Soref, and J. A. Del Alalmo, IEEE J. Quantum Electron. **26**(1), 113 (1990).